INTERNATIONAL CENTER FOR NUMERICAL METHODS IN ENGINEERING

A Methodology for Adaptive Mesh Refinement in Optimum Shape Design Problems

G. Bugeda
E. Oñate

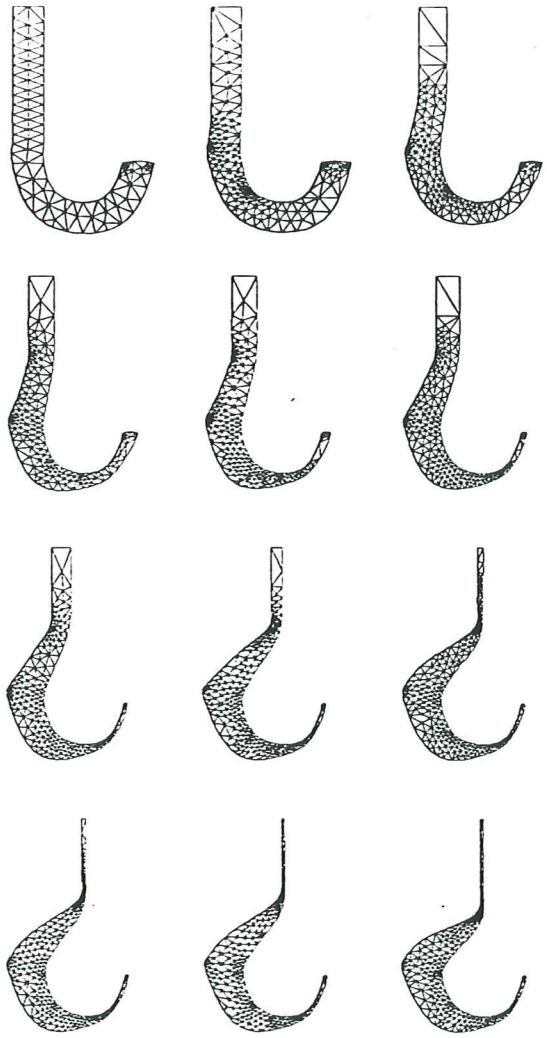

Publicación CIMNE Nº 31, Marzo 1993

A METHODOLOGY FOR ADAPTIVE MESH REFINEMENT IN OPTIMUM SHAPE DESIGN PROBLEMS

G. BUGEDA and E. OÑATE

International Center for Numerical Methods in Engineering
Universitat Politècnica de Catalunya
Módulo C1; Campus Norte UPC; Gran Capitán s/n;08034 Barcelona;Spain

SUMMARY

This work presents a methodology based on the use of adaptive mesh refinement (AMR) techniques in the context of shape optimization problems analyzed by the Finite Element Method (FEM). A suitable and very general technique for the parametrization of the optimization problem using B-splines to define the boundary is first presented. Then, mesh generation using the advancing front method, the error estimation and the mesh refinement criteria are dealt with in the context of shape optimization problems. In particular, the sensitivities of the different ingredients ruling the problem (B-splines, finite element mesh, design behaviour, and error estimator) are studied in detail. The sensitivities of the finite element mesh coordinates and the error estimator allow their projection from one design to the next, giving an "a priori knowledge" of the error distribution on the new design. This allows to build up a finite element mesh for the new design with an specified and controlled level of error. The robustness and reliability of the proposed methodology is checked out with some 2D examples.

1. INTRODUCTION

From a mathematical point of view the treatment of an optimization or an inverse problem can be viewed as the minimization of a function $f(\boldsymbol{x})$ depending on a set of variables $\boldsymbol{x}$ and subjected to some constraints [1,6]. The general form of such a problem is:

$$\begin{array}{lll} minimize: & f(\boldsymbol{x}); \boldsymbol{x} = \{x_i\} & ; i = 1, ..., n \\ with: & \boldsymbol{g}(\boldsymbol{x}) = \{g_j(\boldsymbol{x})\} & ; j = 1, ..., m \\ verifying: & g_j(\boldsymbol{x}) \leq 0 & ; j = 1, ..., m \\ & a_i \leq x_i \leq b_i & ; i = 1, ..., n \end{array} \tag{1}$$

where f is the objective function, x_i are the design variables and g_j are inequality constraints which, for structural problems, are normally expressed in terms of stresses or displacements [1,6]. The values a_i and b_i define lateral constraints. Each set of values $\boldsymbol{x}$ defines one structural design and the problem consists of finding the values of $\boldsymbol{x}$ defining the best design.

The algorithms for the solution of the minimization problem are typically iterative, and they involve the computation of the derivatives (sensitivities) of the objective function and constraints with respect to the design variables [1,6]. Besides, in each step of the process the values of f and $\boldsymbol{g}$ and their sensitivities are needed. In

many cases, as those considered in this work, the computations are performed via a finite element analysis which provides the behaviour of each design, and a methodology to compute the corresponding sensitivities. The definition of each design in terms of the x variables is called "parametrization" of the optimum design problem.

There are many existing codes and different methodologies to solve the optimization problem defined in (1) [6]. However, some problems still remain unsolved in this context, e.g. the inclusion of robust parametrization procedures for definition of each design and the control of the error associated with finite element computations and its influence on the solution of the optimization problem. Usually, once the optimization process is finished there is no guarantee of the accuracy of the final design. Sometimes a more accurate analysis would reveal that the final design is unfeasible, as one or more of the constraints imposed are violated.

With a view towards solving this problem a general methodology for structural shape optimization problems should include the following features:

- general parametrization procedures in order to deal with different structure types with the same structural optimization code. The definition of any design would only need then a small number of design variables.
- easy treatment of boundary conditions.
- easy and general definition of the objective function and constraints.
- automatic, robust and flexible mesh generation.
- accurate and inexpensive estimation of the discretization errors.
- effective, reliable and not too expensive sensitivity analysis.
- efficient optimization procedures.
- automatic adaptive remeshing procedures without a large increase of the total cost.
- control over the quality of the meshes used for each design, i.e., distorted elements should be avoided when significant changes of the structural shape are expected.

In this paper we present a general methodology for optimization problems including all the above mentioned features. In the following sections we describe the parametrization of the optimum design problem, the procedure for automatic mesh generation and error estimation, the sensitivity analysis, and the adaptive remeshing strategy used. In the final part of the paper some examples showing the efficiency of the methodology proposed are presented.

2. THE PROPOSED METHODOLOGY

A flow chart summarizing the proposed methodology is shown in Figure 1. This consists of a series of modules each one corresponding to a specific task. Some of these modules are discussed in detail in the next sections.

Each design step requires to compute the sensitivities of the objective function and constraints. The sensitivity analysis is performed step by step following the same path as the finite element analysis. This path indicates the dependence of each quantity used in the analysis with respect to the rest of the quantities previously employed. For example, the expression of the stiffness matrix depends on the nodal coordinates, so that, following the chain rule for derivatives, the stiffness matrix sensitivities can be expressed in terms of the nodal coordinates sensitivities. Thus, it is necessary to

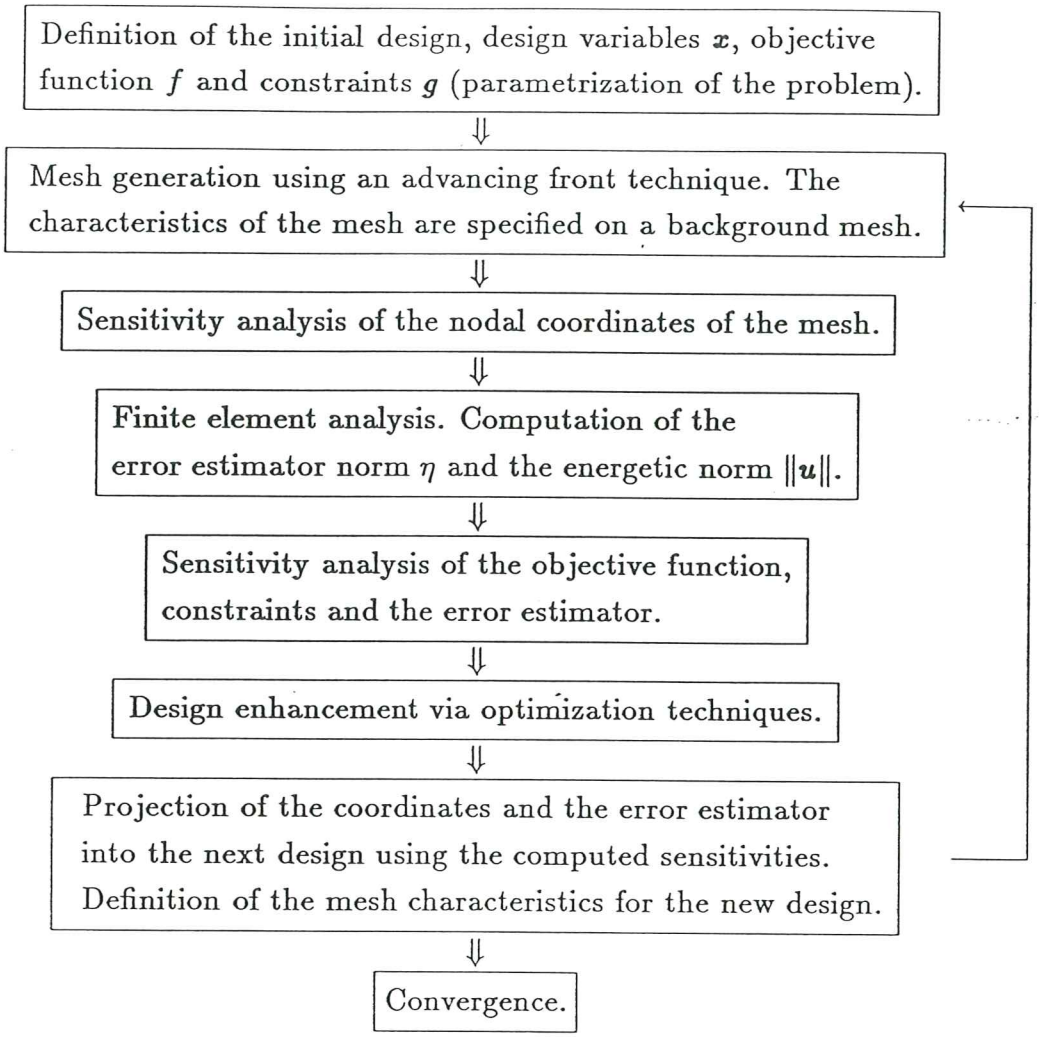

FIGURE 1. General scheme of the proposed methodology.

compute these sensitivities (mesh sensitivities) prior to that of the stiffness matrix sensitivities.

First-order and second-order sensitivity analyses have been used in the implementation of the proposed methodology. The sensitivity analysis provides directional derivatives of any quantity. In the next paragraphs s will denote a unit vector in the design variables space ($x = \{x_1, x_2, ..., x_i, ..., x_n\}$), and derivatives will be computed in the s direction. For instance, to obtain the sensitivities with respect to a specific design variable x_i, s has to be the unit vector corresponding to the x_i direction (i.e. $s = \{0, 0, ..., 1, ..., 0\}$).

The sensitivities of any quantity will be used to project its value from one design into the next one when the design variables are modified. For example, let us assume that $f(x^k)$ is the objective function value at the k-th iteration of the optimization process. If the design variables are modified in the form $x^{k+1} = x^k + \theta^k s^k$, the value of the objective function can be projected into the next design by means of a standard Taylor expansion:

$$f(x^{k+1}) = f(x^k + \theta^k s^k) \approx f(x^k) + \theta^k \frac{\partial f}{\partial s^k} + \frac{1}{2}\theta^{k2} \frac{\partial^2 f}{\partial s^{k2}} \tag{2}$$

The same applies to any other magnitude to be projected.

3. PARAMETRIZATION OF THE PROBLEM

Each design geometry is represented by using "definition points" which specify some interpolation curves. The curves used here are parametric B-splines. The general expression of a closed B-spline for q points is [1,5]:

$$\boldsymbol{r}(t) = \sum_{l=0}^{q} \boldsymbol{r}_l N_{4,l+1}(t) \tag{3}$$

where $\boldsymbol{r}(t)$ is the position vector depending on a parametric variable t. The coordinates of the definition points are recovered using $t = 0, 1, 2, ...$ (see Figure 2). The curve is expressed as a linear combination of $q+1$ normalized fourth order (cubic) B-splines [1,5]. The $\boldsymbol{r}_l$ coefficients are the coordinates of the so called polygon definition points [1,5] and they are found by using the coordinates of the definition points. The degree of continuity of a cubic B-spline is C^2. By using eq. (3), the coordinates of the definition points and some additional conditions about slopes and curvatures, the following equation system can be derived:

$$\boldsymbol{V} = \boldsymbol{N}\boldsymbol{R} \tag{4}$$

where $\boldsymbol{V}$ is a vector containing the imposed conditions at the definition points, $\boldsymbol{N}$ is a matrix containing some terms corresponding to the values of the polynomials that define each B-spline, and the $\boldsymbol{R}$ vector contains the coefficients $\boldsymbol{r}_i$ to be computed. Details of this process can be found in [1,5].

The first and second order sensitivities of $\boldsymbol{R}$ along a direction $\boldsymbol{s}$ in the design variable space are given by:

$$\frac{\partial \boldsymbol{R}}{\partial \boldsymbol{s}} = \boldsymbol{N}^{-1}\left(\frac{\partial \boldsymbol{V}}{\partial \boldsymbol{s}} - \frac{\partial \boldsymbol{N}}{\partial \boldsymbol{s}}\boldsymbol{R}\right) \quad , \quad \frac{\partial^2 \boldsymbol{R}}{\partial \boldsymbol{s}^2} = \boldsymbol{N}^{-1}\left(\frac{\partial^2 \boldsymbol{V}}{\partial \boldsymbol{s}^2} - \frac{\partial^2 \boldsymbol{N}}{\partial \boldsymbol{s}^2}\boldsymbol{R} - 2\frac{\partial \boldsymbol{N}}{\partial \boldsymbol{s}}\frac{\partial \boldsymbol{R}}{\partial \boldsymbol{s}}\right) \tag{5}$$

The derivatives of $\boldsymbol{V}$ with respect the coordinates of the definition points chosen as design variables can be easily computed. Vectors $\partial \boldsymbol{R}/\partial \boldsymbol{s}$ and $\partial^2 \boldsymbol{R}/\partial \boldsymbol{s}^2$ will contain the terms $\partial \boldsymbol{r}_i/\partial \boldsymbol{s}$ and $\partial^2 \boldsymbol{r}_i/\partial \boldsymbol{s}^2$, respectively [1].

Finally, the sensitivities of the coordinates of any point on the interpolation curve corresponding to a constant value of t are obtained by:

$$\frac{\partial \boldsymbol{r}(t)}{\partial \boldsymbol{s}} = \sum_{i=0}^{q} \frac{\partial \boldsymbol{r}_i}{\partial \boldsymbol{s}} N_{4,i+1}(t) \quad , \quad \frac{\partial^2 \boldsymbol{r}(t)}{\partial \boldsymbol{s}^2} = \sum_{i=0}^{q} \frac{\partial^2 \boldsymbol{r}_i}{\partial \boldsymbol{s}^2} N_{4,i+1}(t) \tag{6}$$

4. MESH GENERATION AND SENSITIVITY ANALYSIS

The mesh generation algorithm chosen is the well known advancing front method. This technique is ideal to generate non structured triangular meshes [11,12].

The characteristics of the desired mesh are specified via a background mesh over which nodal values of the size parameter δ are defined and interpolated using the shape functions. The background mesh for the first design has to be defined by hand. For subsequent designs the background mesh will coincide with the mesh projected into this design from the previous one. This projection will be described later.

Once the sensitivities of the coordinates of each boundary node are known, it is also possible to compute the sensitivities of the coordinates of each internal nodal point (mesh sensitivities). These sensitivities are used to asses how the mesh evolves when the design variables change.

There are many different ways to define the evolution of the mesh in terms of the design variables. It is possible to consider a simple analogous elastic medium defining the mesh on movement. This is the case of the "spring analogy" where each element side is regarded as a spring connecting two nodes. The force produced by each spring is proportional to its length. The solution of the equilibrium problem in the spring analogy is simple but expensive and it involves to solve a linear system of equations with two of degrees of freedom per node.

In this work the spring analogy problem has ben solved iteratively using a Laplacian smoothing. This technique is frequently used to improve the quality of non-structured meshes. It consists on the iterative modification of the nodal coordinates of each interior node by placing it at the center of gravity of adjacent nodes. The expression of the new position vector of each node $\boldsymbol{r}_i$ for each iteration is given by:

$$\boldsymbol{r}_i = \frac{\sum_{j=1}^{m_i} \boldsymbol{r}_j}{m_i} \tag{7}$$

where $\boldsymbol{r}_j$ are the position vectors of the m_i nodes connected with the i-th node.

The solution of the spring analogy problem with a prescribed error tolerance requires to check the solution after each smoothing cycle. Taking into account that the described iterative process is only a way to obtain mesh sensitivities, rather than the solution of the equilibrium problem itself, rigorous convergence conditions are not needed. For this reason the number of smoothing cycles to be applied can be fixed a priori. In the examples presented below we have checked that 50 iterations are enough to ensure a good quality of results.

The first-order and higher-order mesh sensitivity analyses along any direction of the design variables space, $\boldsymbol{s}$, are obtained by differentiating eq. (7) with respect to $\boldsymbol{s}$ for each cycle, i.e.

$$\frac{\partial \boldsymbol{r}_i}{\partial \boldsymbol{s}} = \frac{\sum_{j=1}^{m_i} \frac{\partial \boldsymbol{r}_j}{\partial \boldsymbol{s}}}{m_i} \quad , \quad \frac{\partial^2 \boldsymbol{r}_i}{\partial \boldsymbol{s}^2} = \frac{\sum_{j}^{m_i} \frac{\partial^2 \boldsymbol{r}_j}{\partial \boldsymbol{s}^2}}{m_i} \tag{8}$$

5. FINITE ELEMENT ANALYSIS

In this paper we will consider only the solution of structural problems governed by the standard elliptic equations [14]:

$$\boldsymbol{L}\boldsymbol{u} \equiv \boldsymbol{S}^T\boldsymbol{D}\boldsymbol{S}\boldsymbol{u} = \boldsymbol{v} \text{ in } \Omega \tag{9}$$

with appropriate boundary conditions [14]. Applications of the proposed methodology to other elliptic problems like incompressible potential flow models can be found in [4,13].

Discretization of eq. (9) leads to the standard linear system of equations [14]:

$$\boldsymbol{K}\boldsymbol{a} = \boldsymbol{q} \quad with \quad \begin{cases} \boldsymbol{K} = \sum_e \boldsymbol{K}_e \\ \boldsymbol{K}_e = \int_{\Omega_e} \boldsymbol{B}^T\boldsymbol{D}\boldsymbol{B}d\Omega \\ \boldsymbol{q} = \sum_e \boldsymbol{q}_e \\ \boldsymbol{q}_e = \boldsymbol{q}_{\Omega_e} + \boldsymbol{q}_{\Sigma_e} + \boldsymbol{q}_{P_e} \\ \boldsymbol{q}_\Omega = \int_{\Omega_e} \boldsymbol{N}^T\boldsymbol{b}d\Omega \\ \boldsymbol{q}_{\Gamma_e} = \int_{\Gamma_e} \boldsymbol{N}^T\boldsymbol{t}d\Gamma \\ \boldsymbol{q}_{P_e} = \sum \boldsymbol{N}^T\boldsymbol{p} \end{cases} \tag{10}$$

where $\boldsymbol{K}$, $\boldsymbol{a}$ and $\boldsymbol{q}$ denote, as usual, the stiffness matrix, the nodal displacement and the equivalent nodal force vectors. Vectors $\boldsymbol{b}$, $\boldsymbol{t}$ and $\boldsymbol{p}$ correspond to the body, surface and point loads respectively. Matrix $\boldsymbol{B} = \boldsymbol{S}\boldsymbol{N}$ is used to obtain the strains at each point as $\boldsymbol{\epsilon} = \boldsymbol{B}\boldsymbol{a}$ and the constitutive matrix $\boldsymbol{D}$ relates strains with stresses as $\boldsymbol{\sigma} = \boldsymbol{D}\boldsymbol{\epsilon}$.

In our work, nodal stresses $\bar{\boldsymbol{\sigma}}^*$ are recovered using a global least squares smoothing technique [15,16]:

$$\begin{cases} \boldsymbol{\sigma}^* = \sum N_i\bar{\boldsymbol{\sigma}}_i^* = \bar{\boldsymbol{N}}^T\bar{\boldsymbol{\sigma}}^* \\ \bar{\boldsymbol{\sigma}}^* = \boldsymbol{M}^{-1}\boldsymbol{\Phi} \\ \boldsymbol{\Phi} = \sum_e \int_{\Omega_e} \bar{\boldsymbol{N}}^T\boldsymbol{\sigma}d\Omega \\ \boldsymbol{M} = \sum_e \boldsymbol{M}_e \\ \boldsymbol{M}_e = \int_{\Omega_e} \bar{\boldsymbol{N}}\bar{\boldsymbol{N}}^T d\Omega \end{cases} \tag{11}$$

Other procedures for nodal stress recovery, such as the one recently proposed by Zienkiewicz and Zhu [17], can be used.

6. ERROR ESTIMATION

The error associated with each finite element solution is evaluated for each element using the Zienkiewicz and Zhu[15,16] error estimator as:

$$\|e\|_{E_e}^2 \approx \eta_e^2 = \int_{\Omega_e} (\boldsymbol{\sigma}^* - \boldsymbol{\sigma})^T\boldsymbol{D}^{-1}(\boldsymbol{\sigma}^* - \boldsymbol{\sigma})d\Omega \tag{12}$$

The global error estimator η^2 is found by addition of all the elemental

contributions $\eta^2 = \sum_e \eta_e^2$. The energy norm can be defined and estimated from the expression:

$$\|\boldsymbol{u}\|_E^2 = \int_\Omega \boldsymbol{\sigma}^T \boldsymbol{D}^{-1} \boldsymbol{\sigma} d\Omega \approx \int_\Omega \boldsymbol{\sigma}^{*T} \boldsymbol{D}^{-1} \boldsymbol{\sigma}^* d\Omega + \eta^2 = \boldsymbol{a}^T \boldsymbol{K} \boldsymbol{a} + \eta^2 \tag{13}$$

This error estimator has been found to be quite robust, reliable and inexpensive, especially for linear elements. The element sizes for a new mesh are obtained using an adequate remeshing strategy [1–3,8–10]. This issue will be dealt with in a next section.

7. SENSITIVITY ANALYSES OF THE OBJECTIVE FUNCTION, THE CONSTRAINTS AND THE ERROR ESTIMATOR

The objective function will be usually expressed in terms of a cost function which is normally related to the volume of the structure. Constraints are typically related with strains, stresses or displacements. Therefore it is necessary to evaluate the sensitivities of the structural volume, strains, stresses and displacements to compute the sensitivities of the objective function and the restrictions. This requires the computation of the sensitivities of all the magnitudes involved in the analysis.

The exact sensitivity analysis of all the element expressions can be obtained by direct derivation of eqs. (10). This provides the sensitivities of all magnitudes in terms of the mesh sensitivities previously obtained (details of this process are described in references [1,6,7]). The sensitivities of an integral expression are computed after its transformation into the isoparametric domain [1,6,7] which shape does not depend on the design variables. The jacobian of this transformation $|\boldsymbol{J}|$ can be expressed in terms of the nodal coordinates, so that, it can also be differentiated in order to know the integral sensitivities. Using the techniques developed in [6,7] the sensitivities of the element stiffness matrix can be obtained as:

$$\frac{\partial \boldsymbol{K}_e}{\partial s} = \int_{\Omega_\xi} \left[\frac{\partial \boldsymbol{B}^T}{\partial s} \boldsymbol{D} \boldsymbol{B} |\boldsymbol{J}| + \boldsymbol{B}^T \frac{\partial \boldsymbol{D}}{\partial s} \boldsymbol{B} |\boldsymbol{J}| + \boldsymbol{B}^T \boldsymbol{D} \frac{\partial \boldsymbol{B}}{\partial s} |\boldsymbol{J}| + \boldsymbol{B}^T \boldsymbol{D} \boldsymbol{B} \frac{\partial |\boldsymbol{J}|}{\partial s} \right] d\xi_1 d\xi_2 \tag{14}$$

where the sensitivity of the jacobian is:

$$\frac{\partial |\boldsymbol{J}|}{\partial s} = |\boldsymbol{J}| tr \left(\boldsymbol{J}^{-1} \frac{\partial \boldsymbol{J}}{\partial s} \right) \tag{15}$$

In eq. (14) matrix $\boldsymbol{B}$ depends on the nodal coordinates, so that $\partial \boldsymbol{B} / \partial s$ can be obtained from the mesh sensitivities.

Normally, the sensitivities of $\boldsymbol{D}$ will be zero unless a design variable affects the mechanical properties of the material.

This technique allows to obtain first-order and higher-order sensitivities of the stiffness matrix $\boldsymbol{K}$, the nodal forces vector $\boldsymbol{q}$ and of any other integral expression involved in the computations. The detailed expressions for the first-order and higher-order sensitivity analysis can be found in [1,6,7].

Eq. (14) allows to obtain the sensitivities of the displacement vector $\boldsymbol{a}$ as:

$$\frac{\partial \boldsymbol{a}}{\partial s} = K^{-1}\left[\frac{\partial \boldsymbol{q}}{\partial s} - \frac{\partial K}{\partial s}\boldsymbol{a}\right] \quad , \quad \frac{\partial^2 \boldsymbol{a}}{\partial s^2} = K^{-1}\left[\frac{\partial^2 \boldsymbol{q}}{\partial s^2} - \frac{\partial^2 K}{\partial s^2}\boldsymbol{a} - 2\frac{\partial K}{\partial s}\frac{\partial \boldsymbol{a}}{\partial s}\right] \tag{16}$$

Eqs. (16) show that the inverse of the stiffness matrix is needed for the sensitivity computations. If a direct solver is used this matrix has already been factorized and each new sensitivity analysis involves only a new backsubstitution process. Moreover it is not necessary to assemble the sensitivities of the stiffness matrix because they always appear multiplying a vector and these products can be computed in an element-by-element manner.

The strain and stress sensitivities can be computed as:

$$\frac{\partial \boldsymbol{\varepsilon}}{\partial s} = \frac{\partial B}{\partial s}\boldsymbol{a} + B\frac{\partial \boldsymbol{a}}{\partial s} \quad , \quad \frac{\partial^2 \boldsymbol{\varepsilon}}{\partial s^2} = \frac{\partial^2 B}{\partial s^2}\boldsymbol{a} + 2\frac{\partial B}{\partial s}\frac{\partial \boldsymbol{a}}{\partial s} + B\frac{\partial^2 \boldsymbol{a}}{\partial s^2} \tag{17}$$

$$\frac{\partial \boldsymbol{\sigma}}{\partial s} = \frac{\partial D}{\partial s}\boldsymbol{\varepsilon} + D\frac{\partial \boldsymbol{\varepsilon}}{\partial s} \quad , \quad \frac{\partial^2 \boldsymbol{\sigma}}{\partial s^2} = \frac{\partial^2 D}{\partial s^2}\boldsymbol{\varepsilon} + \frac{\partial D}{\partial s}\frac{\partial \boldsymbol{\varepsilon}}{\partial s} + D\frac{\partial^2 \boldsymbol{\varepsilon}}{\partial s^2} \tag{18}$$

The sensitivities of the smoothed stresses are computed in terms of the sensitivities of the mass matrix $\boldsymbol{M}$ and the Φ vector of eq. (11). The techniques discussed above for the integral expressions are also used to compute these sensitivities. Finally, the sensitivities of the smoothed stresses are obtained as:

$$\frac{\partial \bar{\boldsymbol{\sigma}}^*}{\partial s} = M^{-1}\left[\frac{\partial \Phi}{\partial s} - \frac{\partial M}{\partial s}\bar{\boldsymbol{\sigma}}^*\right] \quad , \quad \frac{\partial^2 \bar{\boldsymbol{\sigma}}^*}{\partial s^2} = M^{-1}\left[\frac{\partial^2 \Phi}{\partial s^2} - \frac{\partial^2 M}{\partial s^2}\bar{\boldsymbol{\sigma}}^* - 2\frac{\partial M}{\partial s}\frac{\partial \bar{\boldsymbol{\sigma}}^*}{\partial s}\right] \tag{19}$$

$$\frac{\partial \boldsymbol{\sigma}^*}{\partial s} = \bar{N}^T\frac{\partial \bar{\boldsymbol{\sigma}}^*}{\partial s} \quad , \quad \frac{\partial^2 \boldsymbol{\sigma}^*}{\partial s^2} = \bar{N}^T\frac{\partial^2 \bar{\boldsymbol{\sigma}}^*}{\partial s^2} \tag{20}$$

The same comments about the factorization of the stiffness matrix apply now to the mass matrix.

Following a similar procedure the first-order sensitivity of the error estimator is obtained from eq. (12) as:

$$\begin{aligned}\frac{\partial \eta_e^2}{\partial s} = \int_{\Omega_\xi}\Bigg[&\left(\frac{\partial \boldsymbol{\sigma}^*}{\partial s} - \frac{\partial \boldsymbol{\sigma}}{\partial s}\right)^T D^{-1}(\boldsymbol{\sigma}^* - \boldsymbol{\sigma})|J| + \\ &(\boldsymbol{\sigma}^* - \boldsymbol{\sigma})^T\frac{\partial D^{-1}}{\partial s}(\boldsymbol{\sigma}^* - \boldsymbol{\sigma})|J| + \\ &(\boldsymbol{\sigma}^* - \boldsymbol{\sigma})^T D^{-1}\left(\frac{\partial \boldsymbol{\sigma}^*}{\partial s} - \frac{\partial \boldsymbol{\sigma}}{\partial s}\right)|J| + \\ &(\boldsymbol{\sigma}^* - \boldsymbol{\sigma})^T D^{-1}(\boldsymbol{\sigma}^* - \boldsymbol{\sigma})|J|tr\left(J^{-1}\frac{\partial J}{\partial s}\right)\Bigg] d\xi_1 d\xi_2\end{aligned} \tag{21}$$

In order to use an adaptive mesh refinement strategy it is also necessary to compute the element and total strain energy. The values of this strain energy and

its first and second-order sensitivities can be approximated from the finite element solution as:

$$\|\boldsymbol{u}\|^2_{E_e} \approx \boldsymbol{a}^T \boldsymbol{K}_e \boldsymbol{a} + \eta_e^2 \tag{22}$$

$$\frac{\partial \|\boldsymbol{u}\|^2_{E_e}}{\partial \boldsymbol{s}} \approx \frac{\partial \boldsymbol{a}^T}{\partial \boldsymbol{s}} \boldsymbol{K}_e \boldsymbol{a} + \boldsymbol{a}^T \frac{\partial \boldsymbol{K}_e}{\partial \boldsymbol{s}} \boldsymbol{a} + \boldsymbol{a}^T \boldsymbol{K}_e \frac{\partial \boldsymbol{a}}{\partial \boldsymbol{s}} + \frac{\partial \eta_e^2}{\partial \boldsymbol{s}} \tag{23}$$

$$\begin{aligned} \frac{\partial^2 \|\boldsymbol{u}\|^2_{E_e}}{\partial \boldsymbol{s}^2} \approx & \frac{\partial^2 \boldsymbol{a}^T}{\partial \boldsymbol{s}^2} \boldsymbol{K}_e \boldsymbol{a} + \boldsymbol{a}^T \frac{\partial^2 \boldsymbol{K}_e}{\partial \boldsymbol{s}^2} \boldsymbol{a} + \boldsymbol{a}^T \boldsymbol{K}_e \frac{\partial^2 \boldsymbol{a}}{\partial \boldsymbol{s}^2} + \\ & 2 \frac{\partial \boldsymbol{a}^T}{\partial \boldsymbol{s}} \frac{\partial \boldsymbol{K}_e}{\partial \boldsymbol{s}} \boldsymbol{a} + 2 \frac{\partial \boldsymbol{a}^T}{\partial \boldsymbol{s}} \boldsymbol{K}_e \frac{\partial \boldsymbol{a}}{\partial \boldsymbol{s}} + 2 \boldsymbol{a}^T \frac{\partial \boldsymbol{K}_e}{\partial \boldsymbol{s}} \frac{\partial \boldsymbol{a}}{\partial \boldsymbol{s}} + \frac{\partial^2 \eta_e^2}{\partial \boldsymbol{s}^2} \end{aligned} \tag{24}$$

8. DESIGN ENHANCEMENT

The objective function sensitivities are used to get improved values of the design variables by means of a minimization method. Depending on the optimization algorithm it may be necessary to use second order sensitivities. The design variables corresponding to the improved design are found as:

$$\boldsymbol{x}^{k+1} = \boldsymbol{x}^k + \theta^k \boldsymbol{s}^k \tag{25}$$

where θ^k is an advance parameter.

The direction of change $\boldsymbol{s}^k$ has been obtained here using a BFGS Quasi-Newton method which only requires first order sensitivities of the objective function. The value of θ^k is obtained by a directional second order sensitivity analysis in the $\boldsymbol{s}^k$ direction. The objective function f can be approximated along this direction using a second order Taylor expansion similar to eq. (2) which minimization provides the value of θ^k. Details of this algorithm can be found in [6].

9. PROJECTION TO THE NEXT DESIGN AND DEFINITION OF THE NEW MESH

Once the new design has been defined, the new values of the error estimator, the "energy" and the coordinates of the mesh can be projected from the previous solution into the next design as:

$$(x,y)^{k+1} = (x,y)^k + \theta^k \left(\frac{\partial x}{\partial \boldsymbol{s}}, \frac{\partial y}{\partial \boldsymbol{s}} \right) + \frac{1}{2} \theta^{k2} \left(\frac{\partial^2 x}{\partial \boldsymbol{s}^2}, \frac{\partial^2 y}{\partial \boldsymbol{s}^2} \right) \tag{26}$$

$$\eta^{k+1^k} = \eta^{k^2} + \theta^k \frac{\partial \|e\|^2}{\partial \boldsymbol{s}} + \frac{1}{2} \theta^{k2} \frac{\partial^2 \|e\|^2}{\partial \boldsymbol{s}^2} \tag{27}$$

$$\|u\|_E^{k+1^2} = \|u\|_E^{k^2} + \theta^k \frac{\partial \|u\|_E^2}{s} + \frac{1}{2}\theta^{k^2} \frac{\partial^2 \|u\|_E^2}{\partial s^2} \tag{28}$$

The projected values provide the necessary information to perform a remeshing over the next design, even before any new computation is performed. In that sense, the error estimator computed "a posteriori" is transformed into an "a priori" error estimator.

This projection is very important because it allows the quality control of the mesh for each design prior to any new computation. The projected values are used to create the background mesh information needed to generate the mesh for the new design. This closes the iterative process which will lead to the "enhanced" optimum design after convergence.

The generation of every new mesh in the remeshing procedure requires the definition of a "mesh optimality criterion". In this work a mesh is considered as optimal when the error density is equally distributed across the volume, i.e. when $\|e\|_e^2/\Omega_e = \|e\|^2/\Omega$ is satisfied. The justification of this mesh optimality criterion can be found in [1–3,8–10].

The combination of the mesh optimality criterion and the error estimation allows to define the new element sizes. Previously, it is necessary to define the allowable global error percentage γ as:

$$\gamma = 100\frac{\|e\|}{\|u\|} \approx 100\frac{\eta}{\sqrt{\eta^2 + (a^T K a)^2}} \tag{29}$$

The target error level for each element is:

$$\|e\|_e^t = \frac{\gamma}{100}\|u\|\sqrt{\frac{\Omega_e}{\Omega}} \tag{30}$$

The new element sizes $\bar{h}_e$ can be computed in terms of the old ones h_e using the expression:

$$h = \frac{h_e}{\xi_e^{1/p}} \qquad with \qquad \xi_e = \frac{\|e\|_e}{\|e\|_e^t} \tag{31}$$

where p is the order of the shape function polynomials. For further details see [1–3,8–10].

The value of ξ_e is limited to 1.5 in order to avoid a too fast diminution of the size of the elements in two consecutive iterations. Numerical experiments show that intermediate designs requiring a large number of elements are, often, far away from the optimal one, and it is not useful to dedicate a lot of computational effort to compute them.

10. EXAMPLES

Two application examples are presented below. The first one is a structural shape optimum design problem where the design of a hook is optimized. The second example

shows the application of the presented methodology to an optimum aerodynamic shape problem where incompressible potential flow equations instead of structural equations are used.

10.1 Optimization of a hook

This example consists in the optimization of the shape of a hook in order to minimize its weight. The initial shape, the applied load and the geometry definition points are shown in Figure 3. Twelve points are allowed to move for improvement of the shape, i.e. nine of them can move horizontally, one can move vertically and the rest have been enforced to move along a straight line inclined 45^{o} (see Figure 3).

A parabolic vertical load has been applied over the inner part of the hook with a resulting load of 630 Kg. The material properties are: Young modulus E=2100000 Kg/cm^2 and Poisson ratio ν=0.3. A plane stress model with 6 node triangular elements has been used. The global error level has been limited to 1%.

The objective function is the weight of the hook. The maximum value of the Von Mises stresses have been constrained to 2000 Kg/cm^2. This constraint has been applied to all the nodes placed along the boundary. The minimum thickness of the spike of the hook has been limited to 0.50 cm.

The algorithm converges after 130 iterations. Figure 4 shows the successive meshes and the designs corresponding to iterations 0, 10, 20, 30, 40, 50, 60, 75, 90, 105, 120 and 130. It can be observed how the optimization process displaces the vertical part of the hook until it coincides with the resultant of the load forces. This is due to the absence of bending moments over this part and thus its width can be considerably reduced. The curved part of the hook is thicker because of bending action producing high stresses on the boundaries.

The evolution of the objective function is presented in Figure 5. After an initial increase of weight to obtain a feasible design there is a fast drop with a good behaviour of the optimization algorithm. The initial weight of 167 Kg is reduced to 82 Kg.

The evolution of the global percentage of error and the number of elements for each mesh are presented in Figures 6 and 7 respectively. Figure 6 shows how the global percentage of error is maintained below the prescribed 1% limit after the two first iterations. The whole problem has taken around 3.0 CPU hours on a Silicon Graphics Indigo R4000 workstation.

The sensitivity analysis corresponding to each design variable requires around an additional 10% of the CPU cost of the standard FEM analysis. The second-order sensitivity analysis needs an additional 10% CPU time. For this particular example (twelve design variables) this means that the total CPU cost for each iteration of the optimization process takes around 230% of the cost of a single FEM analysis. This cost can be compared with that of a standard optimization approach using a complete adaptive remeshing procedure for each design. This will require at least two FEM analyses for each design and a complete sensitivity analysis for the last one. This means that each new design would require at least 330% of the CPU cost of a single FEM analysis. These simple figures show that the use of the methodology presented can save more than one third of the cost of a standard optimization process linked to an adaptive refinement strategy.

10.2 Flow inverse problem

This application example corresponds to one of the test cases defined for the workshop on "Optimum Design in Aerodynamics" held in Barcelona on June 1992 [18]. A detailed description of the application of the presented methodology to uncompressible flow problems can be found in [4]. Note that there is a big analogy between the incompressible potential flow and the structural models studied here due to the linear elliptic nature of both.

This problem consists in recovering the Korn airfoil at an angle of attack 0°. The target pressure coefficient C_p^{target} has been obtained by a direct computation of the Korn airfoil with a finite element code using adaptive remeshing and a maximum global error of 0.1%. The infinite boundary is placed a distance of 10 chords from the profile. The initial design corresponds to a NACA 64A410 profile.

The inverse problem has been solved using a minimization approach. The cost functional to be minimized has been defined as:

$$f = \int_0^2 (C_p(x) - C_p^{target})^2 ds \tag{32}$$

This integral is extended around the profile and the integration variable is the arc s and not the x coordinate so that all the boundary is equally weighted. If the x variable is used, the cost function tends to put more weight on the medium part of the profile and less on the edges.

The geometry of each design has been defined using 25 design variables. These variables are the y coordinates of 25 points distributed around the profile which are used to interpolate a B-spline. Figure 8 shows the initial shape and the finite element mesh of 158 quadratic triangles (6 nodes) used for the initial design. The 25 points used to define the shape of each design are all the nodes lying on the profile in Figure 8 with the exception of the trailing edge which is fixed. The maximum global error has been limited to 0.1% of the total potential norm.

The iterative process has converged after 50 iterations. The final shape and the final mesh of 495 quadratic triangles can be observed in Figure 9. The whole problem has taken around 3.5 hours of CPU on a Silicon Graphics Indigo R4000 workstation.

The evolution of the normalized cost functional during the process can be seen in Figure 10. Figure 11 shows the evolution of the L2 difference norm between the solution profile and the design profile. This norm has been computed as the L2 difference norm between each design and the final one since no information on the exact definition of the Korn airfoil using the 25 control points was available. In fact it is not possible to define exactly the Korn airfoil using the 25 interpolating points. Figure 12 shows the evolution of the global error during the minimization process. Figure 13 shows the evolution of the number of finite elements used for each design. Figure 14 shows the C_p distributions for the initial profile, the target profile and the last design obtained.

Figures 10 and 11 show a good convergence of the minimization process. The cost functional has been reduced almost 2 orders of magnitude in 50 iterations.

The global error involved in the finite element computations has been controlled. In fact it is very low compared with the 0.1% limitation. This is because the error is concentrated around the profile, but a little bit far away the flow is almost uniform and the error is almost null. This explains why the global error is small. The important

issue, in fact, is how the error is distributed around the profile. Figure 9 shows how the mesh concentrates many more elements around the leading edge where the gradients of the potential are higher.

The comparison between the target and the computed C_p values shown in Figure 14 is quite good although some differences are still noticeable. On the other hand Figure 10 shows that the process seems to be converged, and it is not possible to get a solution closer to the target one. The reasons are that probably it is not possible to get a better definition of the Korn airfoil using a B-splines interpolation with 25 points. In fact the computations over the Korn airfoil have shown that it is extremely sensible to little changes in its shape. In order to get a better final solution it would be necessary to use more design variables to enhance the B-spline interpolation, but this would considerable increase the total cost.

11. CONCLUSIONS

A new methodology for the resolution of optimization and inverse problems has been developed and assessed. This methodology is able to optimize the design and the analysis mesh together in order to produce a final design computed with a proper mesh.

Good quality results are obtained using a single mesh for each design without any remeshing. This considerably reduces the additional cost of the mesh control.

The presented methodology has provided excellent results for all the application examples analyzed leading to an accurate final solution with a good final mesh.

12. ACKNOWLEDGMENTS

The authors acknowledge the support of the Commission of the European Communities DG-XII through the BRITE/EURAM project "Optimum Design in Aerodynamics".

13. REFERENCES

[1] Bugeda, G. "Utilización de técnicas de estimación de error y generación automática de mallas en procesos de optimización estructural." Ph. D. Thesis - Universitat Politècnica de Catalunya (1990) (In Spanish).

[2] Bugeda, G. and Oñate, E., "New adaptive techniques for structural problems", First European Conference on *Numerical Methods in Engineering*, Brussels, Belgium, September, 1992.

[3] Bugeda, G. and Oñate, E., "Adaptive mesh refinement techniques for aerodynamic problems", in *Numerical Methods in Engineering and Applied Sciences.* H. Alder, J. C. Heinrich, S. Lavanchy, E Oñate & B. Suárez (Eds.), CIMNE-Barcelona 1992.

[4] Bugeda, G., Oñate, E. and Joannas, D., "Aerodynamic Shape Optimization using Automatic Adaptive Remeshing.", published in *Notes on Numerical*

Fluid Mechanics. Proceedings of the Optimum Design Final BRITE/EURAM Workshop, Vieweg-Verlag, to appear 1993.

[5] Faux, I. D. and Pratt, M. J. "Computational Geometry for Design and Manufacture.", Edited by Ellis Horwood Limited, 1987.

[6] Navarrina, F. "Una metodología general para optimización estructural en diseño asistido por ordenador." Ph. D. Thesis - Universitat Politècnica de Catalunya (1987) (In Spanish).

[7] Navarrina, F., Bendito, E. and Casteleiro M. "High order sensitivity analysis in shape optimization problems." - *Computer Methods in Applied Mechanics and Engineering, vol. 75, pp. 267-281 (1989)*

[8] Oñate, E., Castro, J. and Kreiner, R., "Error estimations and mesh adaptivity techniques for plate and shell problems", presented at the *3rd. International Conference on Quality Assurance and Standards in Finite Element Methods*, Stratford-upon-Avon, England, 10–12 September, 1991.

[9] Oñate, E. and Castro, J., "Adaptive mesh refinement techniques for structural problems", published in *"The Finite Element Method in the 90's. A book dedicated to O. C. Zienkiewicz"*, E. Oñate, J. Periaux and J. Samuelsson (Eds.), Springer-Verlag&CIMNE, Barcelona 1991.

[10] Oñate, E. and Bugeda, G., "A Study of Mesh Optimality Criteria in Adaptive Finite Element Analysis" to be published in *"Engineering Computations"*

[11] Peraire, J. "A Finite Element Method for Convection Dominated Flows." - Ph. D. Thesis - University College of Swansea (1986)

[12] Peraire, J., Morgan, K. and Peiró, J. "Unstructured finite element mesh generation and adaptive procedures for CFD." - *AGARD FDP: Specialist's Meeting, Loen, Norway (1989)*

[13] Pironneau, O. "Méthodes des éléments finis pour les fluides." Masson 1988.

[14] Zienkiewicz, O.C. and Taylor R. L., "The Finite Element Method. Fourth Edition. Volume 1. Basic Formulation and Linear Problems." Mc Graw Hill 1989.

[15] Zienkiewicz, O.C. and Zhu, J.Z., "A simple error estimator and adaptive procedure for practical engineering analysis", *Int. Num. Meth. Engrg.*, 24, 337–357, 1987.

[16] Zienkiewicz, O.C., Zhu, J.Z., Liu, I.C., Morgan, K. and Peraire, J., "Error estimates and adaptivity from elasticity to high speed compressible flow", in J.R. Whiteman, ed., MAFELAP 87, 483–512, Academic Press, New York, 1988.

[17] Zienkiewicz, O.C. and Zhu, J.Z. - "The superconvergent patch recovery and *a posteriori* error estimates. Part 1: The recovery technique." - *International Journal for Numerical Methods in Engineering, vol. 33, pp. 1331-1364 (1992)*

[18] Brite Euram 1082 partners, "Workshop on Selected Inverse and Optimum Design Problems. Definition of Test Cases" (1992).

LIST OF FIGURES

NOTE: In order to reduce the number of pages for this paper the figures can be reduced.

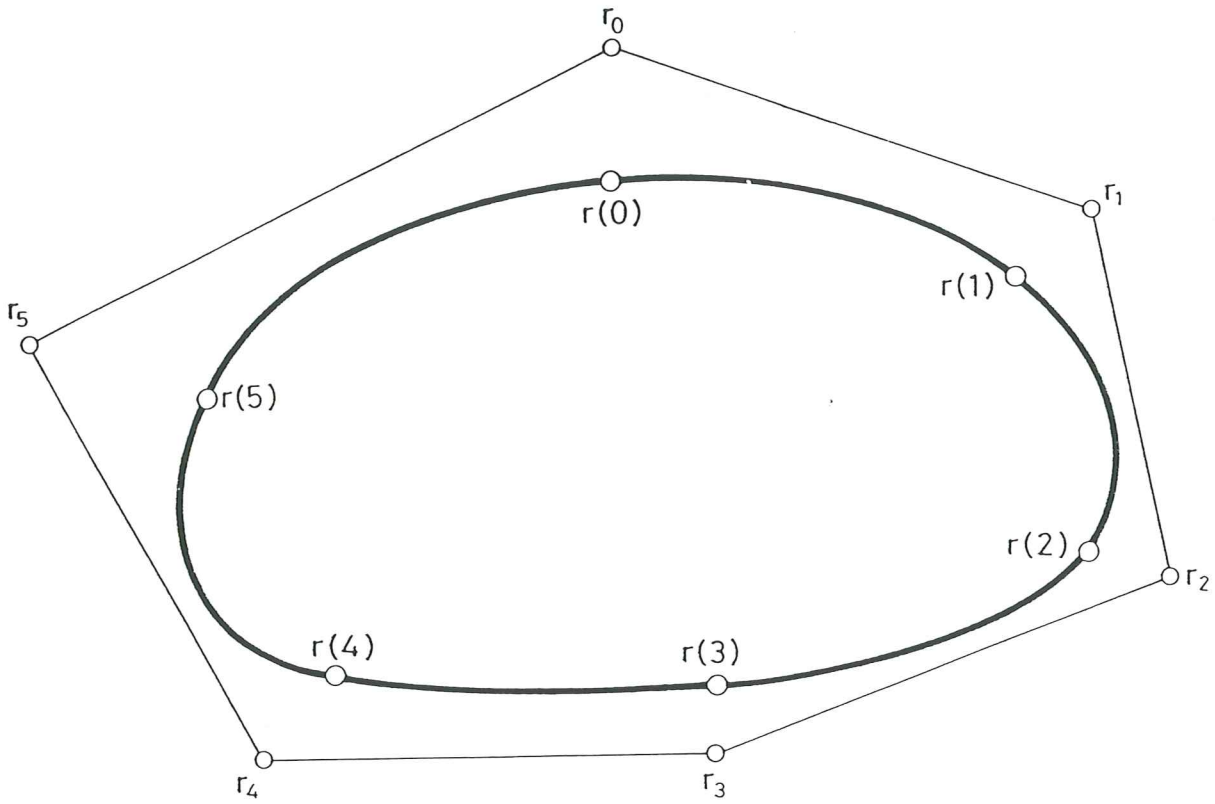

Figure 2. Definition points and polygon definition points of a B-spline.

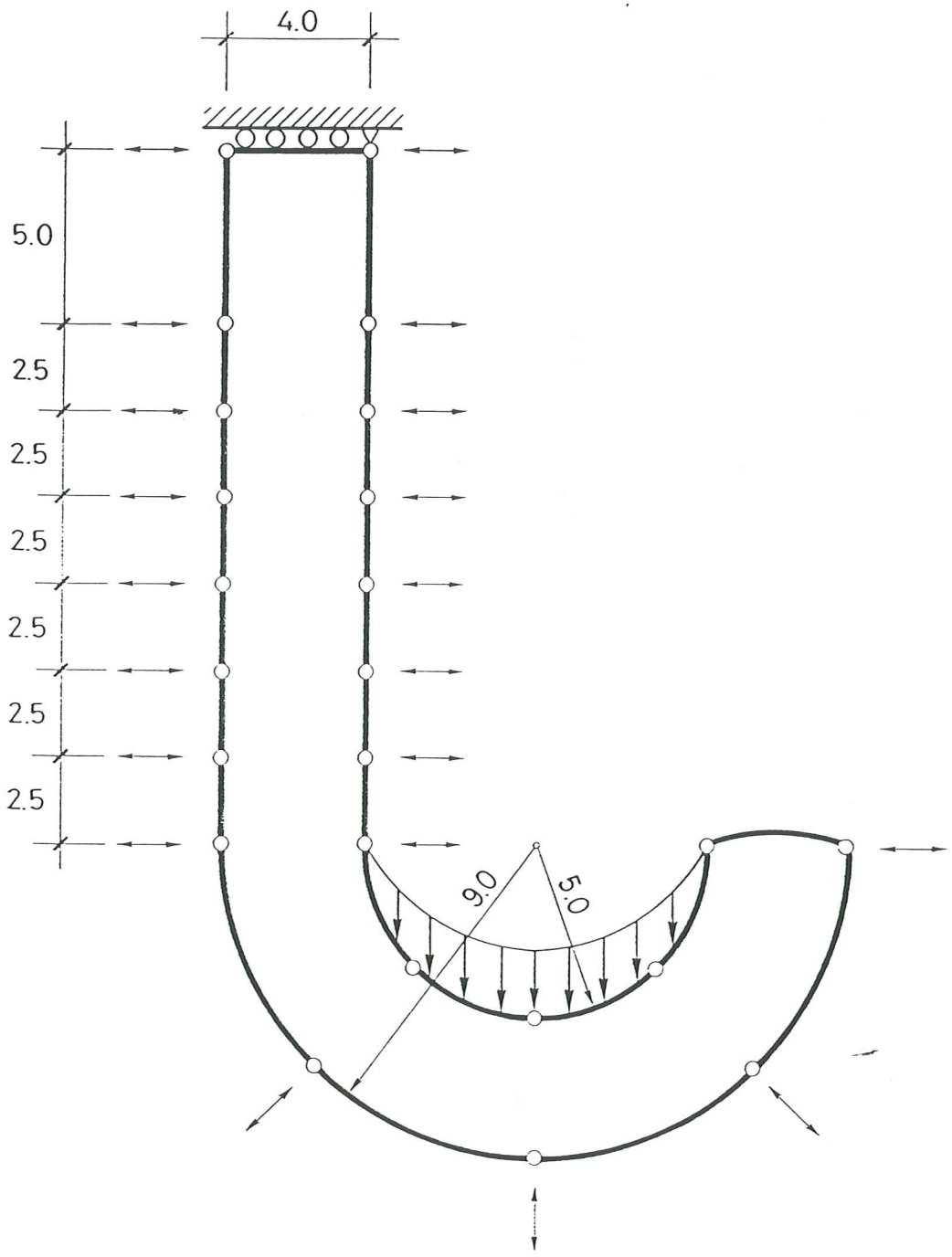

Figure 3. Hook optimization problem. Initial shape and parametrization.

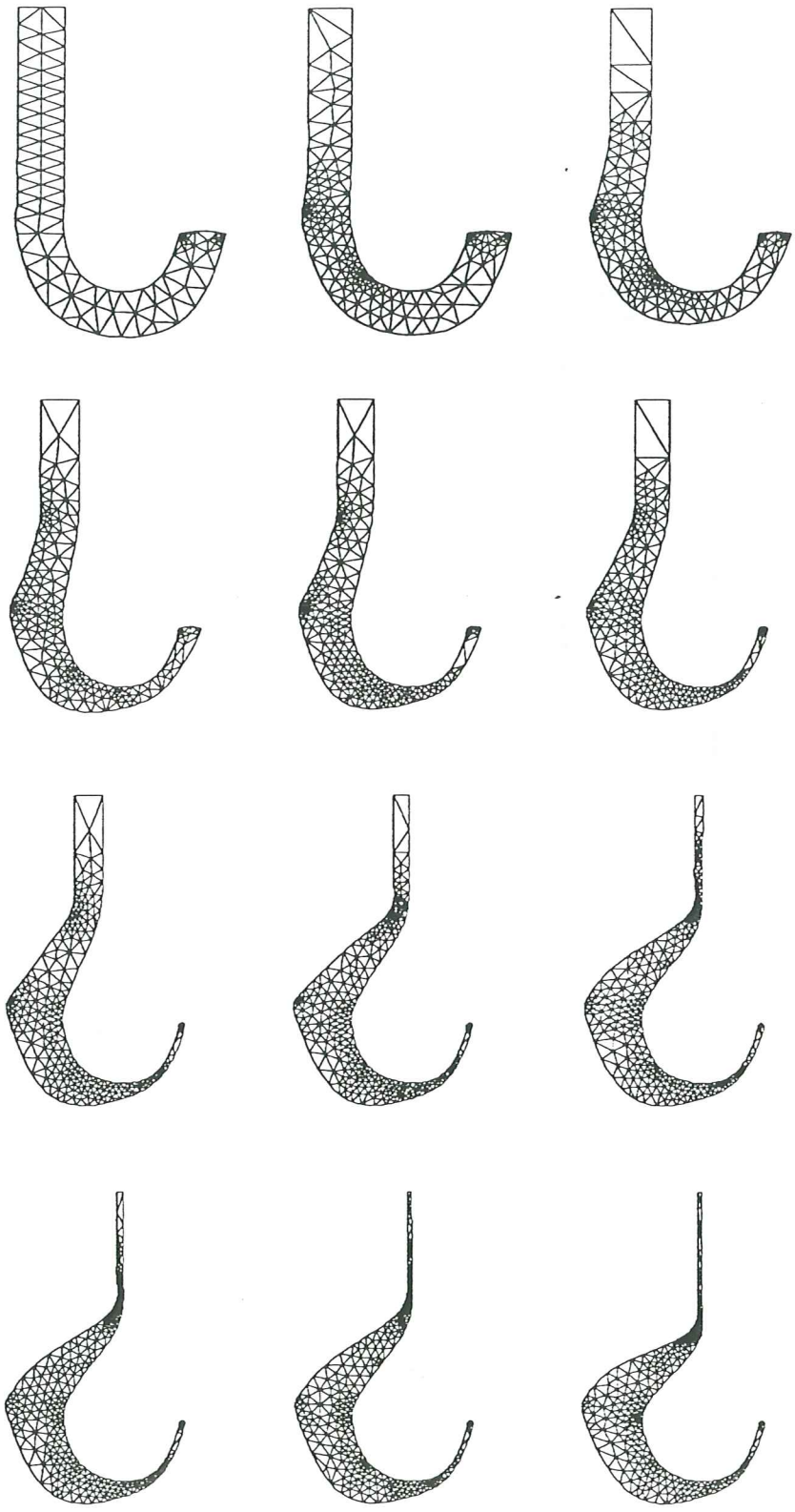

Figure 4.Hook optimization problem. Successive meshes and designs for iterations 0, 10, 20, 30, 40, 50, 60, 75, 90, 105, 120 and 130.

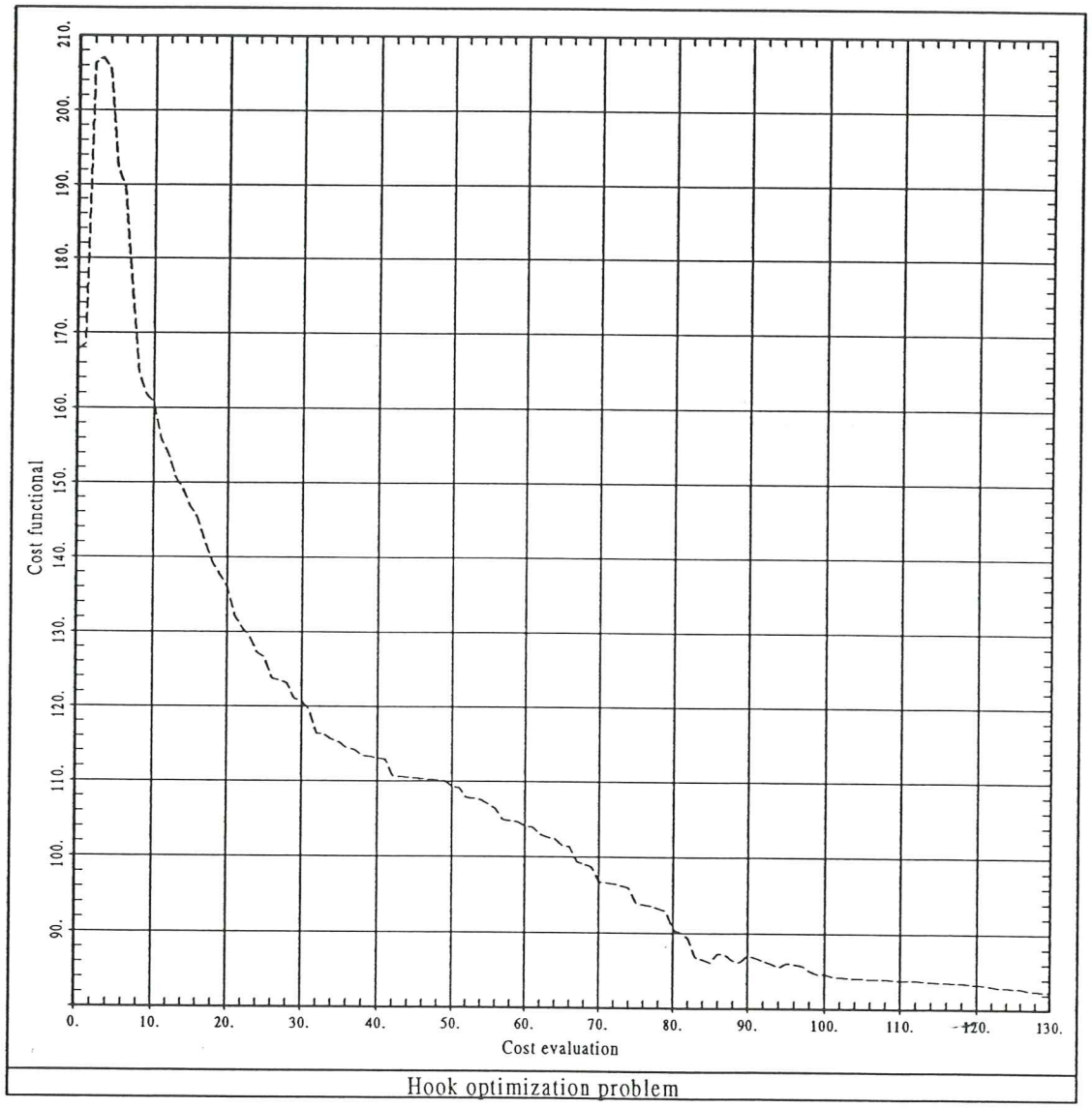

Figure 5. Hook optimization problem. Evolution of the objective function.

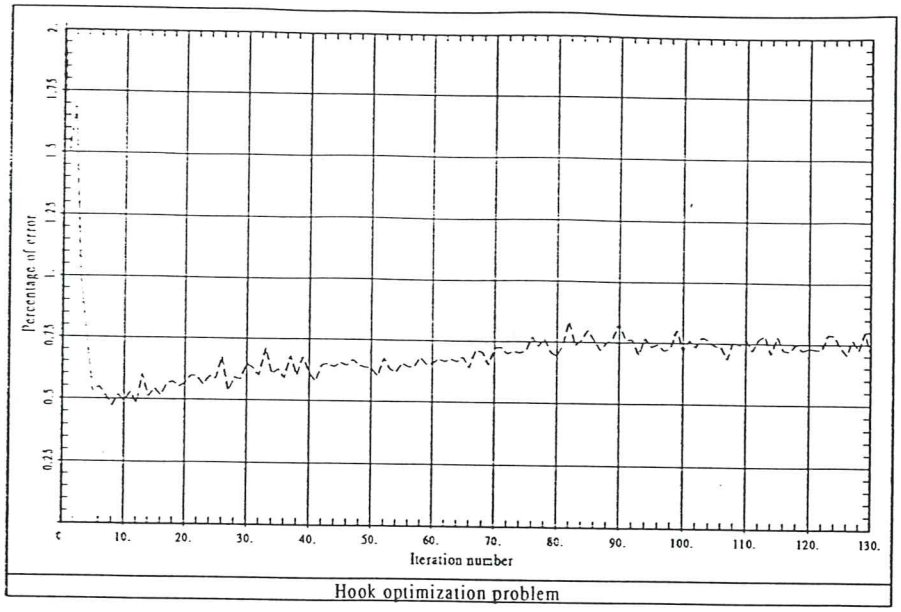

Figure 6.Hook optimization problem. Evolution of the global percentage of error.

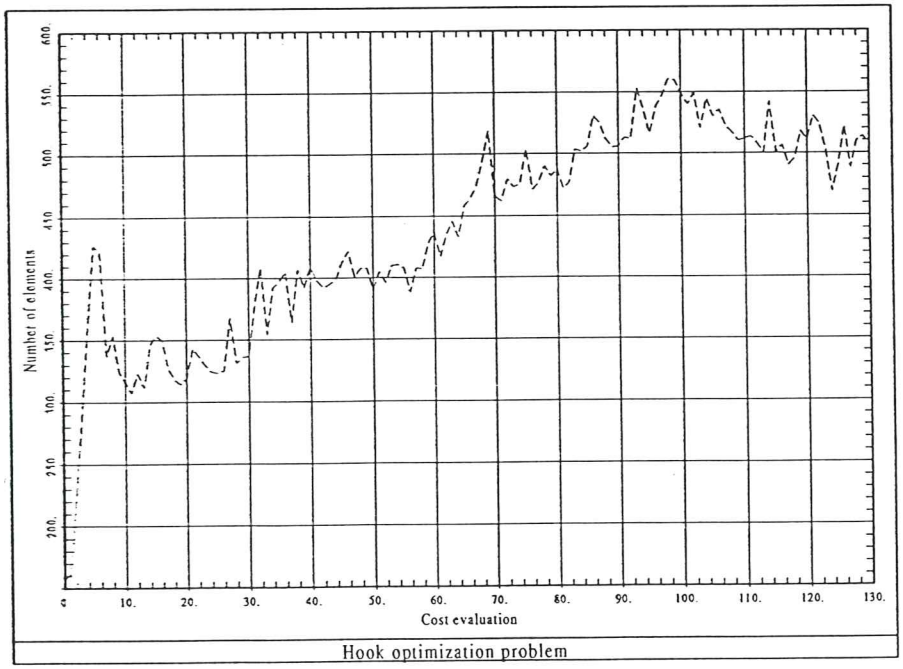

Figure 7.Hook optimization problem. Evolution of the number of elements of each mesh.

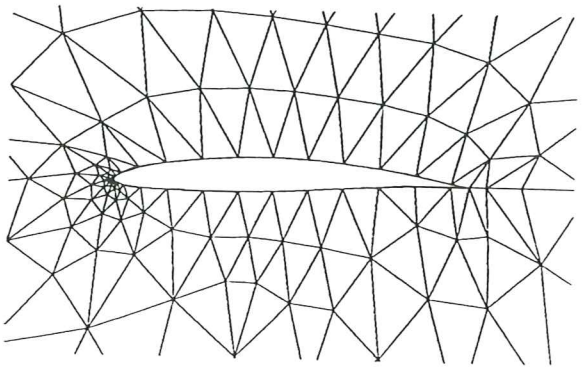

Figure 8. Korn reconstruction problem. Initial shape, initial mesh and definition of the design

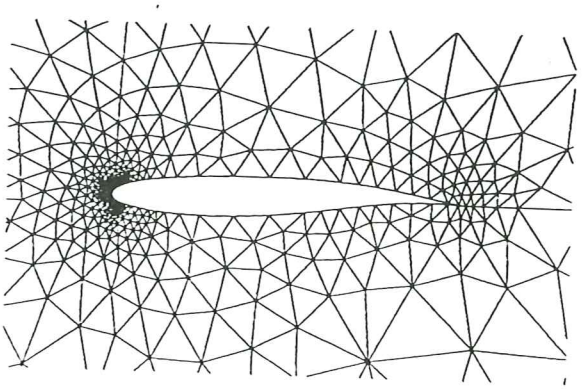

Figure 9. Korn reconstruction problem. Final shape and final mesh.

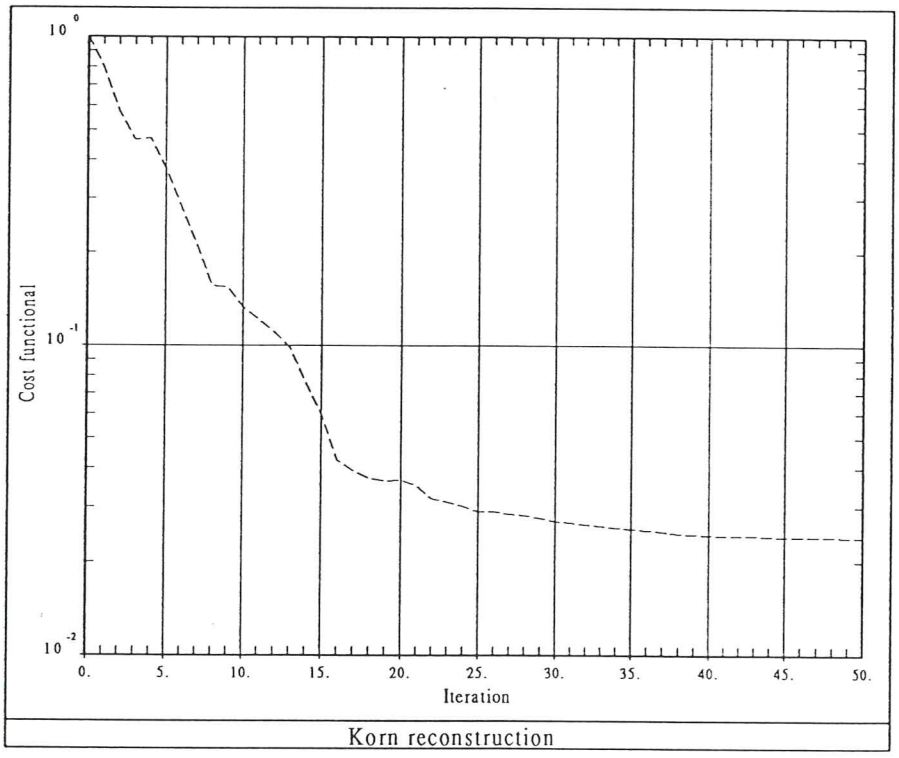

Figure 10.Korn reconstruction problem problem. Evolution of the objective function

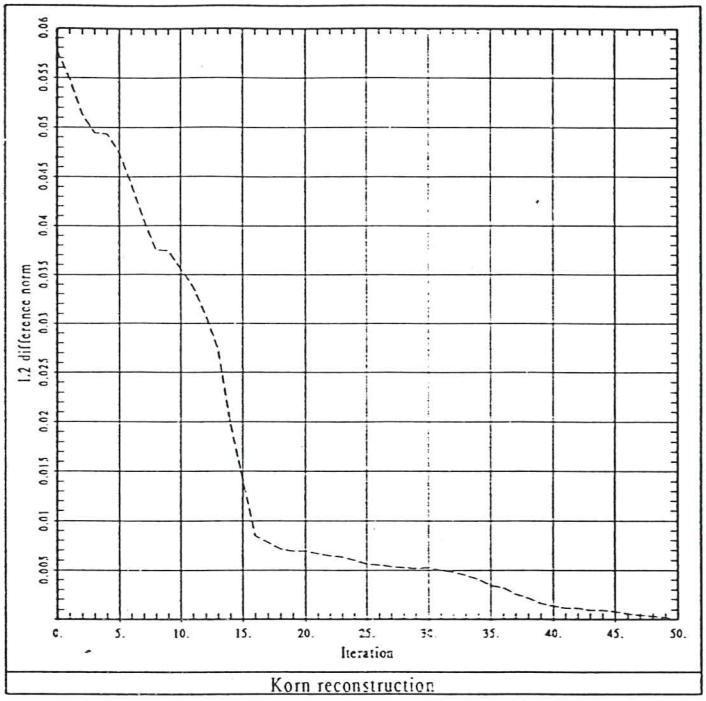

Figure 11.Korn reconstruction problem problem. Evolution of the global L2 difference norm.

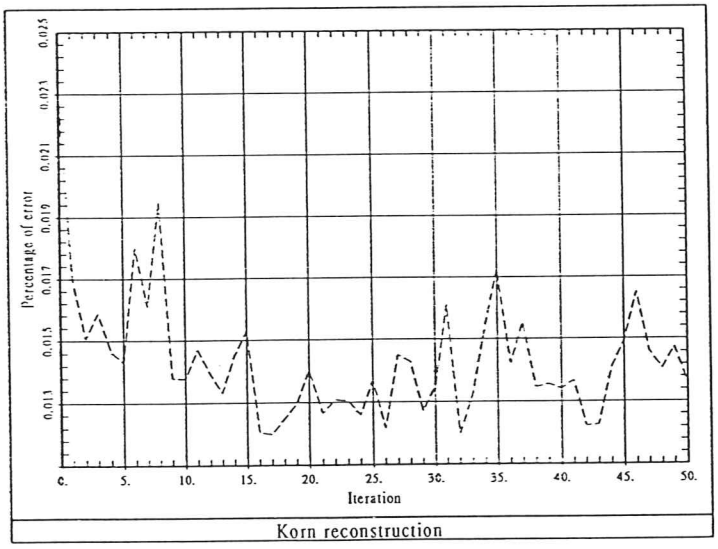

Figure 12.Korn reconstruction problem problem. Evolution of the global percentage of error.

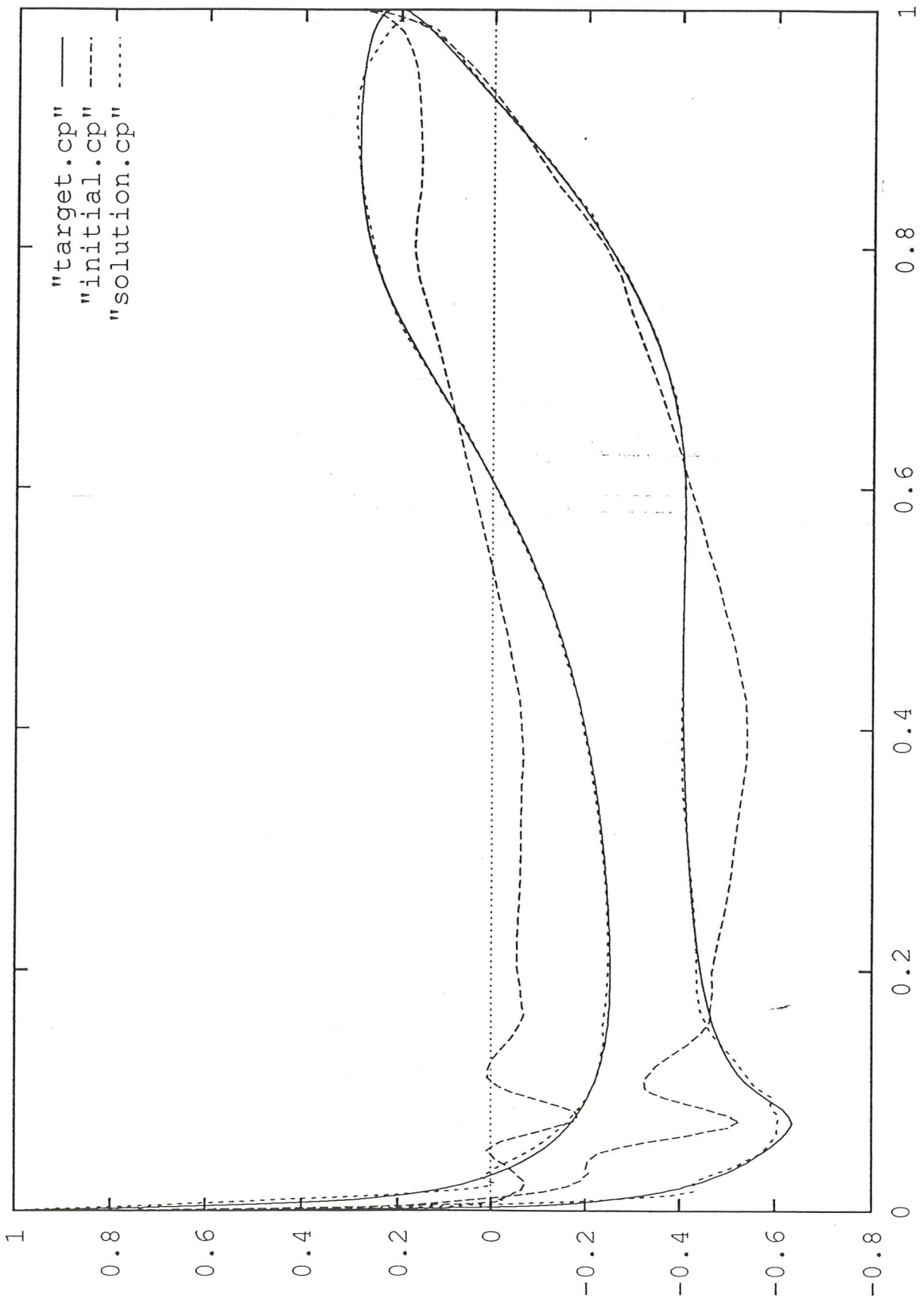

Figure 14.Korn reconstruction problem problem. Distribution of C_p for the initial profile, the target design and the computed design.

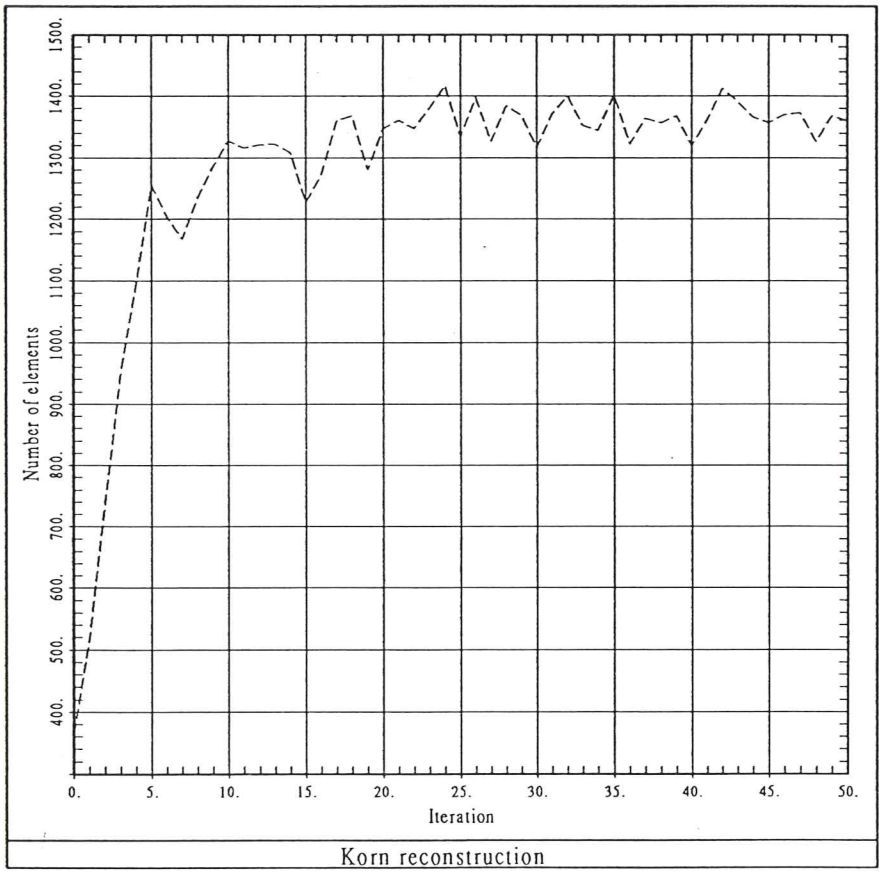

Figure 13.Korn reconstruction problem problem. Evolution of the number of elements of each mesh.

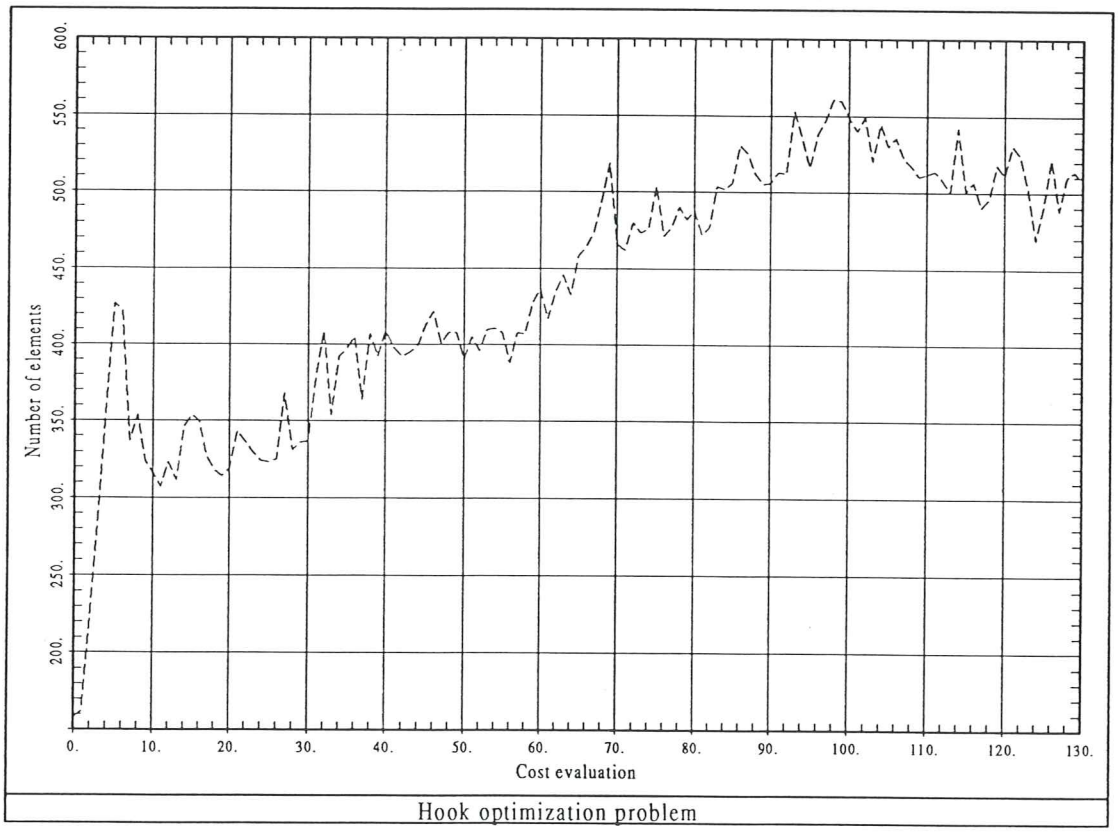

Figure 7.Hook optimization problem. Evolution of the number of elements of each mesh.

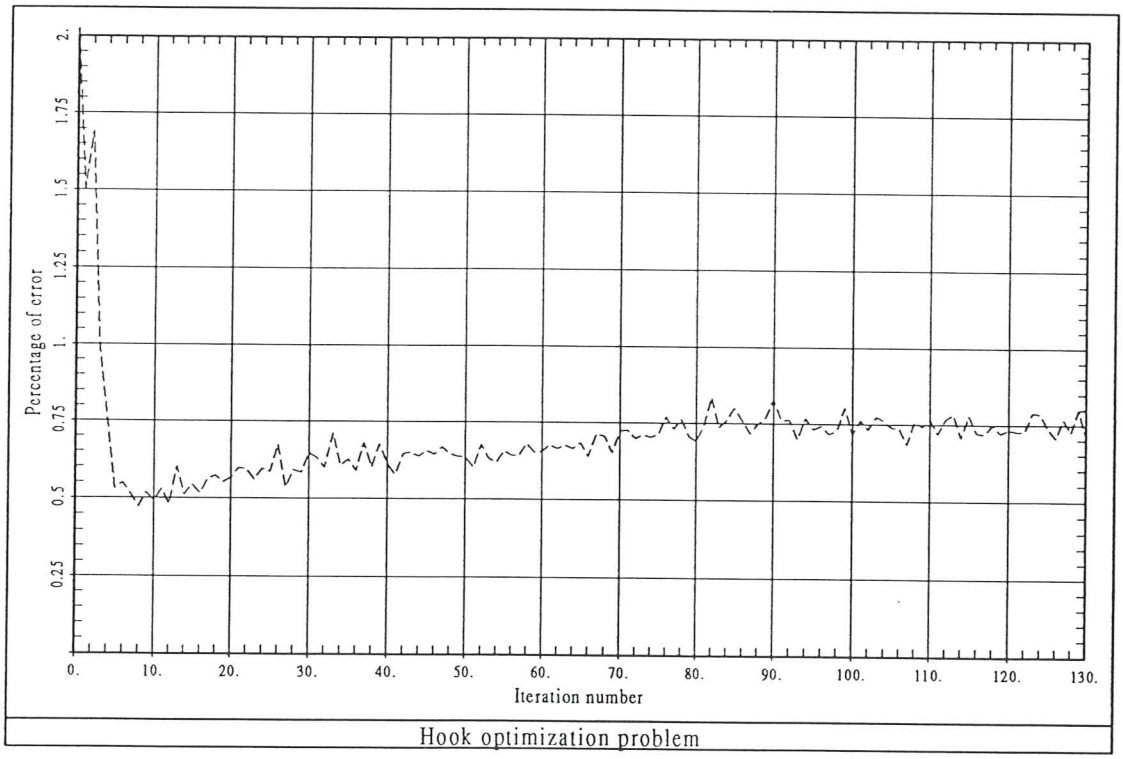

Figure 6.Hook optimization problem. Evolution of the global percentage of error.

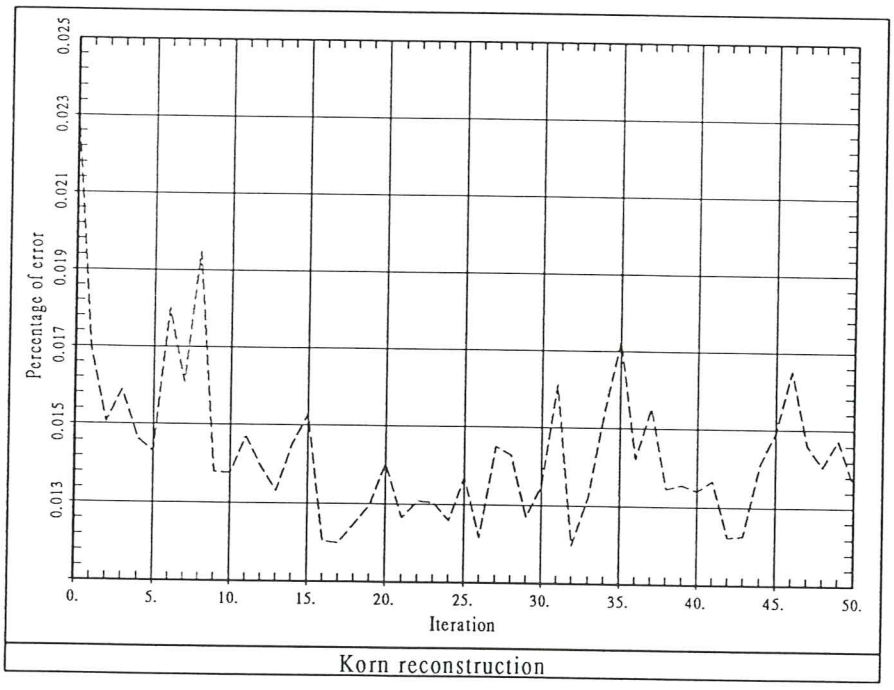

Figure 12.Korn reconstruction problem problem. Evolution of the global percentage of error.

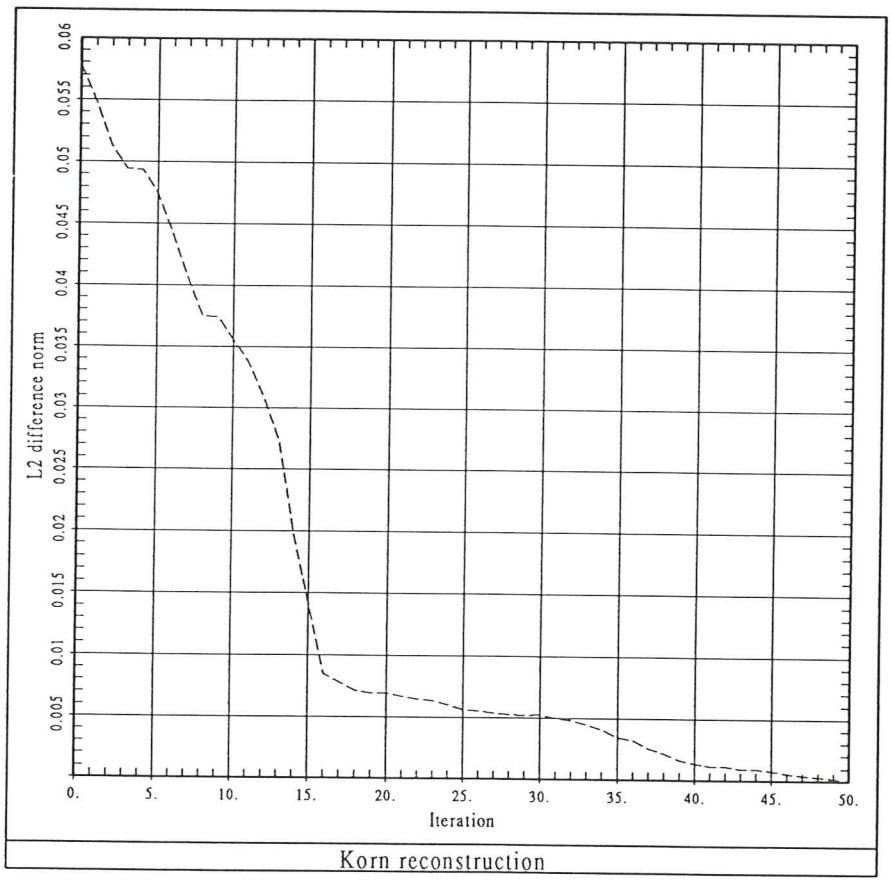

Figure 11.Korn reconstruction problem problem. Evolution of the global L2 difference norm.